http://dx.doi.org/10.1016/j.jallcom.2021.160104

Re-precipitation mechanisms of the γ′ phase with sphere, near-sphere, cubic, octets and finally-dendrite in as-cast Ni-based superalloys

Hao Yu [a], Zhaotian Wang [a], Baoyun Zhang [a], Yongquan Ning [a*], M.W. Fu [b]

[a] *School of Materials Science & Engineering, Northwestern Polytechnical University, Xi'an 710072, P.R. China*

[b] *Department of Mechanical Engineering, The Hong Kong Polytechnic University, Hung Hom, Kowloon, Hong Kong, P.R. China*

*CORRESPONDING AUTHOR:

Tel: +86 29 88493744

Fax: +86 29 88492642

E-mail: ningke521@163.com; luckyning@nwpu.edu.cn (Y.Q. Ning)

ABSTRACT:

The morphology and size distribution of γ' phases have a significant impact on the thermal processing and manufacturing of components made of superalloys and their service performance under adverse conditions. The homogenization treatment of as-cast superalloys ingot is the first modulation of the morphology, size distribution and other characters of γ' phase. Therefore, investigation on the re-precipitation mechanism of γ′ phase is of critical theoretical value and engineering significance. In this research, the morphology evolution and size distribution of re-precipitation γ′ phase in an as-cast Ni-based superalloy during homogenizing treatment were investigated extensively and systematically. The re-precipitation mechanism of γ′ phase with sphere, near-sphere, cubic, octets and finally-dendrites was identified under various cooling conditions. The γ′ phase size is increased while the nucleation density is decreased with the cooling conditions changing from air cooling (AC) to furnace cooling (FC). The γ′ phase stability during growth was discussed and the reprecipitation γ′ phase is generated from a refine spherical shape at fast cooling condition (AC); while irregularity growth even splitting happened at slow cooling condition (FC). The findings help understand the re-precipitation mechanism of the γ′ phase of Ni-based superalloys and provide a basis for controlling of the microstructure and tailoring of the properties of the alloys.

Keywords:

Re-precipitation mechanism; γ′ phase; Ni-based superalloys; Sphere, near-sphere, cubic, octets and finally dendrites; Phase stability

1. Introduction

Ni-based superalloys are extensively used in making turbine discs in jet-engine due to their excellent strength, ductility, fatigue resistance and oxidation resistance at elevated temperature [1]. The outstanding mechanical properties are closely related to the internal microstructure, which is a combination of a FCC γ matrix and a coherent $L1_2$-ordered Ni_3(Al, Ti) particles (γ′ phase) [2-5]. The microstructure evolution of the Ni-based superalloys in hot processing is completely dependent on various processing parameters including solution temperature, soaking time, and cooling rate, etc. [1]. Therefore, it is crucial to understand and determine the morphology and size distribution of γ' phases. Depending on the cooling rate, the morphology of these particles varies from simple spheres over cubes, octocubes, and eventually to the complex structures, such as octodendrites and dendrites [3]. The lattice misfit is considered to be the main reason for a large variety of dissimilar morphologies [4-11].

To understand the details of the formation of γ′ phases, many investigations have been done to know more about the morphology of the γ′ phases and different morphologies were identified [12]. Dendritic shape γ′ phases have been observed when the cooling rate was slowly [12-14]. The lattice mismatch between γ matrix and γ′ phase depends on the morphology of the γ′ phases [15]. When the lattice mismatch is positive, the γ′ cuboids get coarsened along the direction of the applied stress. However, the γ′ cuboids become coarsened along the vertical direction to the direction of the applied stress when the lattice mismatch is negative [16]. In addition, the lattice mismatch also influences the γ′ phase directional coarsening rate [12, 16]. According to the conducted experiment and simulation [17-21], the

γ′ phases are initially spheres and, as becoming coarsened, they grow into cubes and then are split into eight smaller cuboids (octets). After splitting, the coherent strain energy is released and the dendritic shape γ′ phases begin to form [22]. Furthermore, the precipitation behavior and mechanisms of γ′ phases during the cooling process have been extensively studied. In the continuous cooling process, the generated γ′ phases in Rene 88 DT are strongly dependent on cooling rates [23]. After solutionizing in the single phase field, a monomodal size distribution of refined γ′ phases with a high nucleation density and non-equilibrium compositions can be obtained under fast cooling conditions [23-25]. In contrast, a bimodal size distribution or in some cases even a multimodal size distribution of γ′ phases is observed under the relatively slower cooling rate [23-25, 26]. A.R.P. Singh et al [27] developed a mechanistic understanding of the process of multiple nucleation bursts. It leads to the formation of multiple generations of γ′ phases during the continuous cooling. These multiple nucleation bursts, on the other hand, are generated via the continuously increasing thermodynamic driving force for nucleation. These processes are closely related to the undercooling [24, 25]. At lower undercooling, lower driving force for nucleation with high diffusivity levels enables the formation of the primary γ′ phase. However, high undercooling facilitates the supersaturation of γ′ forming elements and the thermodynamic driving force results in the formation of the secondary or tertiary γ′ phase with a high nucleation density. These mechanisms were studied and discussed by using the phase field modeling [27]. In addition, the experimental superalloy in this research is a newly developed cast-wrought Ni-based superalloy for its superior mechanical properties at high temperatures (700-750 °C) and the good properties-versus-cost balance due to its recycling and forging ability [28-30]. The

mechanical properties of this superalloy are very sensitive to the solution heat-treatment and strongly depend on γ′ phases [30]. Therefore, it is crucial to have an in-depth understanding and physical insight into the process and mechanism of the re-precipitation γ′ phases of this alloy.

In this research, the homogenization treatments were conducted at the γ′ super-solvus temperature under various conditions. The process of secondary γ′ phases re-precipitated from single γ phase-field was thoroughly explored and discussed. The γ′ phase morphology transformed from sphere to near-sphere, cubic, octets and finally dendrites under various cooling condition. The re-precipitation mechanisms of the γ′ phase were then identified and the γ′ phase stability during growth under various cooling conditions was discussed. The researches thus help understand the re-precipitation mechanisms of the γ′ phase of this unique Ni-based superalloys during homogenization treatment and provide a basis for determination of the process for homogenizing treatment of as-cast Ni-based superalloys and tailoring of re-precipitation and microstructures of the alloys.

2. Material and experimental procedure

The experimental material is an innovative cast and wrought Ni-based superalloy of the Ni-Co-Cr type, which went through vacuum induction-melting, electroslag remelting and followed by vacuum arc-remelting. Table 1 shows the chemical composition and Fig. 1 presents the initial microstructure of the experimental superalloy. It reveals that the typical dendritic microstructure of the as-received superalloy with the secondary dendrite spacing of 56.6 μm. Element segregation occurs when the alloy with high Ti content and the γ + γ′ eutectic reaction happens with the continuous increase of the Ti content in the interdendritic

liquid phase. Moreover, the γ′ phase of the as-cast superalloy at different locations was identified. Its morphology is a typical butterfly shape. The sizes of the γ′ phase in the dendritic arm region and the interdendritic region are 1.125 and 0.75 μm, respectively. It reveals that the size of γ′ phase is different and the distribution is uneven at different locations of the experimental superalloy.

Table 1 Chemical composition of the Ni-based superalloy

Ni	Fe	Co	Cr	Mo	W	Al	Ti	Nb	B	C	Zr
Base	4	8.5	15.7	3.1	2.7	2.25	3.4	1.1	0.01	0.015	0.03

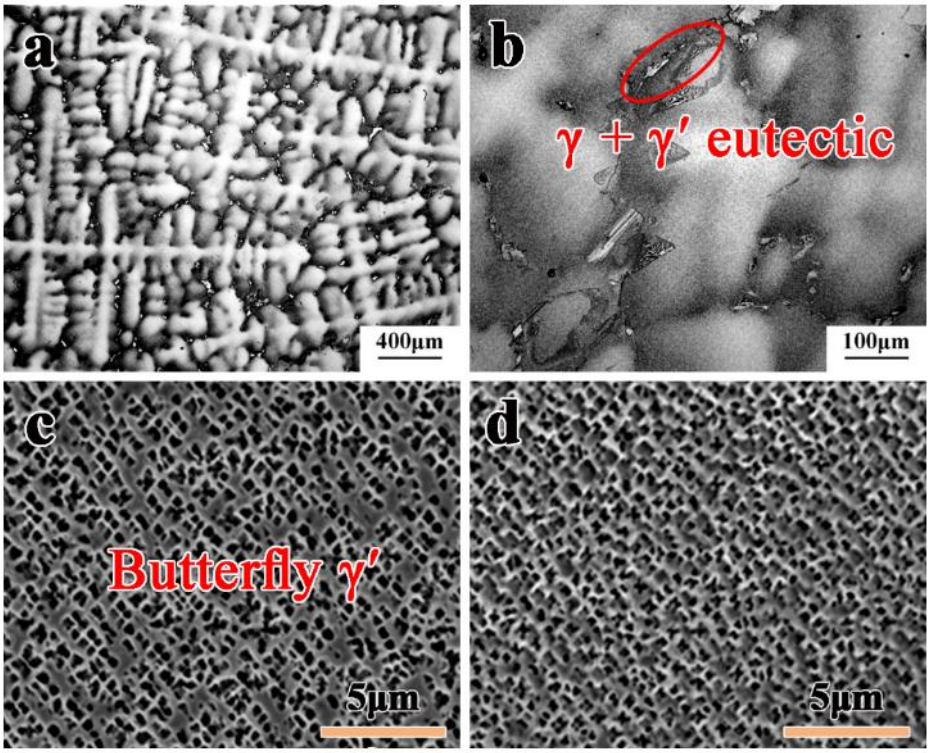

Fig. 1. Typical microstructure of the experimental Ni-based superalloys: (a) dendritic microstructure; (b) γ + γ′ eutectic phase; (c) and (d) butterfly γ′ phase at the dendrite-arm and the interdendritic.

Homogenization samples with 10 mm×14 mm×14 mm in size were cut from the edge of ingot. The parameters of homogenization was generated according to the dissolution

temperature of the γ′ phase. Fig. 2(a) displays a DSC diagram obtained by heating from room temperature (RT) to 700 ℃ at a constant rate of 20 ℃/s, and then from 700 to 1200 ℃ at 10 ℃/s. The figure shows there is an endothermic peak around 1110 ℃, and peak A indicating the dissolution of primary γ′ phase at around 1115 ℃. It should be noted that the γ′ phase dissolution is affected by the combination of heating temperature and soaking time. Fig. 2(b) shows the γ′ phase is almost completely dissolved after homogenization treatment at the temperature of 1110 ℃ with soaking time of 15 h. Above all, the γ′ phase solvus temperature is identified to be about 1110 ℃.

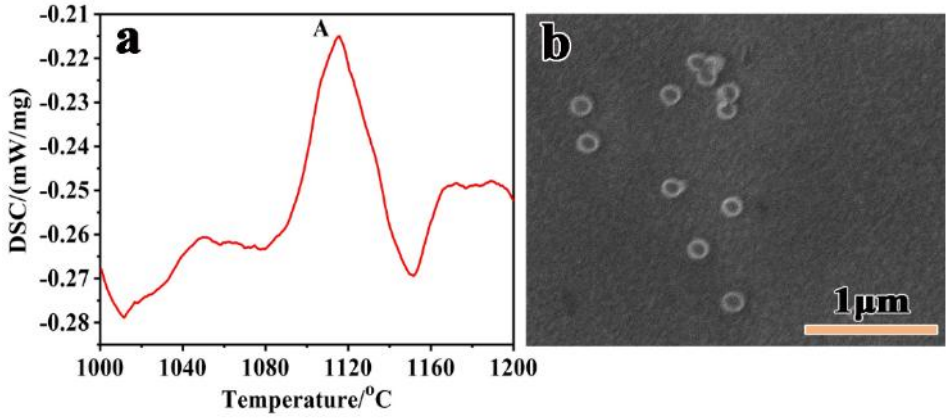

Fig. 2. (a) DSC diagram obtained by heating from room temperature (RT) to 1200 ℃; (b) the γ′ phase after homogenization treatment at temperature of 1110 ℃ with soaking time of 15 h.

The homogenization treatments were conducted in a resistance furnace at the temperatures of 1110, 1130, 1160, and 1190 ℃ with the soaking times of 15, 30, 45 and 60 h. The homogenized samples were then cooled down by furnace cooling (FC), slowing cooling in insulating asbestos (SC), air cooling (AC) and water quenching (WQ). WQ cooling condition reveals the γ′ phase is almost completely dissolved at the experimental temperature (from 1110 to 1190 ℃). The cooling rate of AC, SC and FC is determined to be about

250~300, 60~80 and 4 ℃/min, respectively. It should be highlighted that the determined cooling rates of AC and SC cooling conditions has error in measurement process due to the drop of temperature during the samples taken out from high temperature box resistance furnace. Upon homogenization treatment, all specimens were separated into two parts for microstructure examination. For optical microscope (OM) examination, the samples were etched in a solution of 10 mL HCl+10 mL CH_3CH_2OH+0.5 g $CuCl_2$ at room temperature. For scanning electron microscope (SEM) observation, the samples were etched using two different methods to reveal the γ′ phase characteristics. The first method was electroetched in a mixture of 45% H_2SO_4+42% HNO_3+13% H_3PO_4, with electrolytic etching parameters as 3.5 V and 3-5 s. The second method was electroetched with 150 mL H_3PO_4+10 mL H_2SO_4+15 g CrO_3 for 4-10 s at room temperature. Morphology of the γ′ phases was conducted using TESCAN SEM in the secondary electron (SE) or In-beam mode. OM and SEM images were analyses by using Image-Pro-Plus software. The mean equivalent diameter of each particle was measured in order to measure the γ′ phase size. The secondary γ′ phase partied size distribution (more than 100 γ′ phases were measured) and particle number density were determined by Image-J software. In addition, the measurements of the γ′ phase size are related to the γ′ phase morphology. For sphere and near-spherical, the γ′ phase size is its diameter; while the size is the mean of the length and the width for cubic, octets and dendrites shape. Moreover, the γ′ phase characteristics were also identified by transmission electron microscope (TEM). The compositions of the γ matrix and the γ′ phase were analysed by using an energy dispersive spectroscopy detector equipped on the TEM.

3. Effect of homogenizing parameters on the morphology and size

distribution of the re-precipitation γ' phase

Fig. 3 shows the γ′ phase of the studied superalloy under the homogenization treatment at the temperature of 1160 ℃ with the soaking time of 30 h, and then cooled down by FC. Two types of γ′ phases were visible, which can be defined based on the average size, morphology and nucleation density. The secondary γ′ precipitate with a relatively large size, irregular shape and low nucleation density, is shown in Fig. 3(a). The dendritic and octets phases were measured to have the mean equivalent diameters of 742.7 and 420.2 nm, respectively. Since the γ′ particles initially grew and then split during cooling process upon homogenization treatment, there is also a small number of near-spherical γ′ phase. The tertiary γ′ precipitate with a relatively small size, spherical shape and high nucleation density, as shown in Fig. 3(b). It precipitated around the secondary γ′ phase and was measured to have the mean equivalent diameter ranged from 30 to 50 nm. In addition, it was found that the size, morphology and distribution of the γ' phase have a huge difference under various conditions upon homogenization treatment. As well known, homogenization treatment is dependent on various factors, mainly including homogenization temperature, soaking time and cooling condition. Therefore, the influence of these three homogenizing parameters on the microstructure evolution is a focus to be discussed.

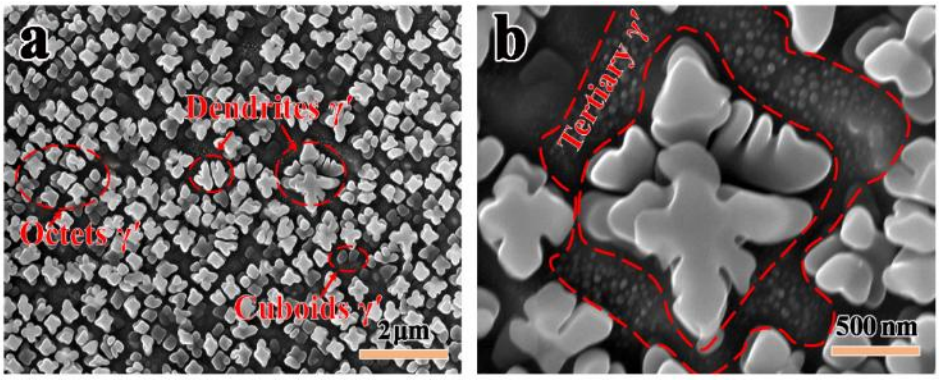

Fig. 3. Two types of γ′ phases upon the homogenization treatment: (a) cuboids, octets and dendrites shape secondary γ′ phases; (b) tertiary γ′ phases distributed around the secondary γ′ phase.

Fig. 4 shows the effect of homogenization time on the morphology, size and distribution of the γ′ phases at the temperature of 1160 ℃ with different homogenization soaking times. As shown in Fig. 4(a), the γ′ phase is a mixture of octets and near-spherical when the homogenization soaking time is 15 h. The size of γ′ phase is quite similar and the distribution is more uniform with the increase of the soaking time. When the homogenization soaking time approaches 60 h, the γ′ phase is almost all octets. The detailed statistics analyses are presented in Table 2 and show that the secondary γ′ phase gets smaller with the decrease of soaking time. With the soaking time of 15 h, the average size of γ′ phase is 296 nm, and it is about 339 nm when the soaking time is about 60 h.

Fig. 5 presents the particle size distribution (PSD) of γ′ phase homogenized at the temperature of 1160 ℃ with different homogenization soaking times. The relative frequency and cumulative frequency with the γ′ phase size histograms were obtained. It can be seen that the peak values of each histogram are close to the statistics results presented in Table 2. The size of γ′ phase has a unimodal distribution for all the conditions. When the soaking time is 15 h, the range of γ′ phase diameter (about 140-580 nm) is wider than that of the soaking time of 60 h (about 200-460 nm). It reveals that the distribution of γ′ phase is more uniform with the increase of soaking time. When homogenizing treatment was performed at the γ′ super-solvus temperature and the soaking time was increased, the γ′ phase dissolved completely. This is beneficial to the uniform distribution of the re-precipitation γ′ phase. In addition, it should be highlighted that the quantification of the γ′ phase has an error in statistical analysis of phase

size due to the limit of SEM.

Table 2 The size statistics of γ′ phase upon homogenization treatment at the temperature of 1160 ℃ with various soaking times

Temperature/℃	Time/h	Phase size (nm)
1160	15	296
	30	308
	60	339

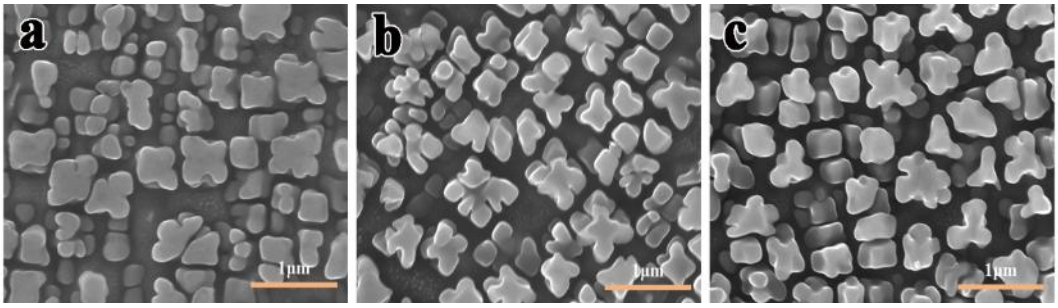

Fig. 4. The γ′ phases of the studied alloy homogenized at the temperature of 1160 ℃ with different homogenization soaking times: (a) 15 h; (b) 30 h; (c) 60 h.

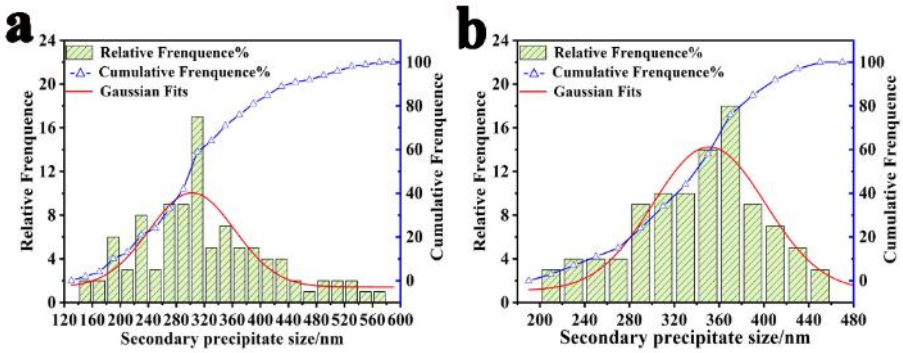

Fig. 5. Secondary γ′ precipitates size distribution plot of the alloy homogenized at the temperature of 1160 ℃ with different soaking times: (a) 15 h; (b) 60 h.

Fig. 6 presents the octets γ′ phases of the studied alloy under different homogenization temperatures with soaking time of 60 h. With the increase of homogenization temperature, the morphology of the γ′ phase did not change much. The detailed statistics analyses are listed in Table 3 and reveal that the γ′ phase size is apparently increased with the homogenization temperature. At the homogenization temperature of 1110 ℃, the average size of γ′ phase was 306 nm, while it became 397 nm when the homogenization temperature approached 1190 ℃.

The relative frequency and cumulative frequency with the secondary γ′ precipitate size histograms were obtained, as shown in Fig. 7. The peak value of each histogram is also closely to the statistics results presented in Table 3. The above analysis shows that homogenization temperature has an important effect on the γ′ phase size. With the increase of the homogenization temperature, the size of secondary γ′ precipitate is increased.

Table 3 The size statistics of γ′ phase at various temperatures with the soaking time of 60h

Temperature/℃	Time/h	Phase size (nm)
1110		306
1160	60	339
1190		397

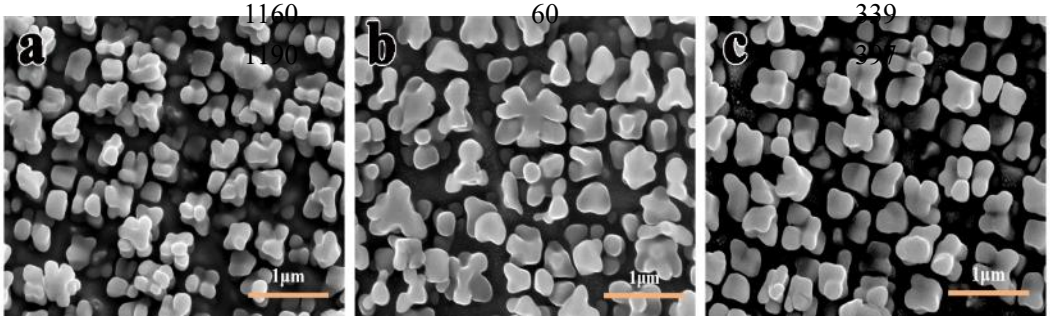

Fig. 6. The γ′ phases of the studied alloy at different homogenization temperatures with the soaking time of 60 h: (a) 1110 ℃; (b) 1160 ℃; (c) 1190 ℃.

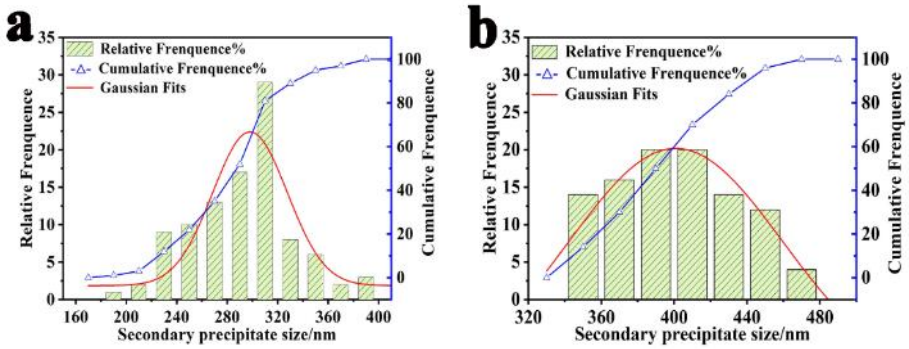

Fig. 7. Secondary γ′ phases size distribution plot of the samples at different homogenization temperatures with soaking time of 60 h: (a) 1110 ℃; (b) 1190 ℃.

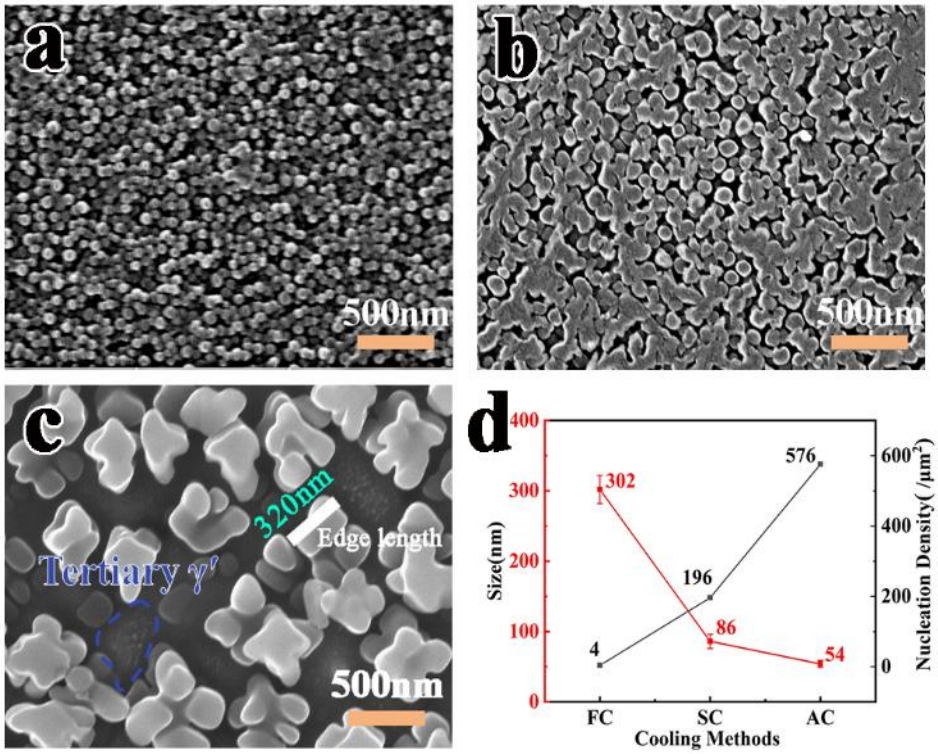

Fig. 8. Typical microstructures of the re-precipitation γ′ phases under various cooling conditions: (a) AC; (b) SC; (c) FC; (d) the size (red line) and nucleation density (black line) of the γ′ phases under various cooling methods.

Fig. 8 shows the morphology and size distribution of γ′ phases under different cooling conditions. The microstructure of the γ′ phase is significantly affected by the cooling conditions and is transformed from sphere to near-sphere, octets shape with the change of the cooling rate. When the cooling condition was AC, the sphere shape γ′ phase was formed. When the cooling condition was SC, the γ′ phase was changed from sphere to near-spherical. With the decrease of cooling rate and the cooling condition was FC, the γ′ phase was mostly the octets. Fig. 8(d) shows size distribution of the γ′ phase under various cooling conditions. The detailed statistics analyses reveal that the γ′ phase size at FC is about 302 nm, about six times the phase size at AC. The nucleation density of the γ′ phase at FC is about 4/μm^2, far

less than the nucleation density of the γ′ phase at AC. The γ′ phase with low nucleation density under slow cooling condition. This would result in the lower total coherent strain energy and thus the coarsening γ′ phases. In fact, the secondary γ′ precipitates are transformed from sphere to near-spherical, cube, octets and dendrites with the slow cooling rate.

The microstructure and distribution of γ′ phases under two different cooling conditions are shown in Fig. 9. It is found that the sphere γ′ phases are distributed randomly under AC cooling condition. When the cooling condition was FC, a large number of octets shape γ′ phases and some cuboids particles existed. Cuboidal γ′ phases distributed along <100> direction and it is revealed that there was a strong interaction between the γ′ phases, as shown in Fig. 9(b). For Ni-based superalloys, the orientation relationship can be described by: $\{100\}_{\gamma}//\{100\}_{\gamma'}$ and $<010>_{\gamma}//<010>_{\gamma'}$. The γ′ phases often align along the elastically soft <100> direction to keep the system at a state with the minimum strain energy [1]. Slow cooling rate (FC) promoted the diffusion of solution atoms, thus the γ′ phases forming elements had sufficient time to reach the interface of the phases and beneficial to the octets γ′ phases formation. These γ′ phases are instable and with apparent concaves at the edge [31]. This is due to the fact that with the growth of the precipitates, the elastic lattice strain is increased as well and far outweighs the reduced interfacial energy [32]. Fig. 9(d) presents the dislocation pile-up at the interface of the γ/γ′. It is found that some γ′ phases had lost the coherency with γ matrix but most of them are still coherent. For tertiary γ′ phases, the cooling condition is irrelevant to its morphology. No tertiary γ′ phases were found under the fast cooling condition (AC). However, lots of dense and fine tertiary γ′ phases were observed in the matrix corridors for the slow cooling rate (FC), and mostly tertiary γ′ phases are sphere

with the size of 30-50 nm.

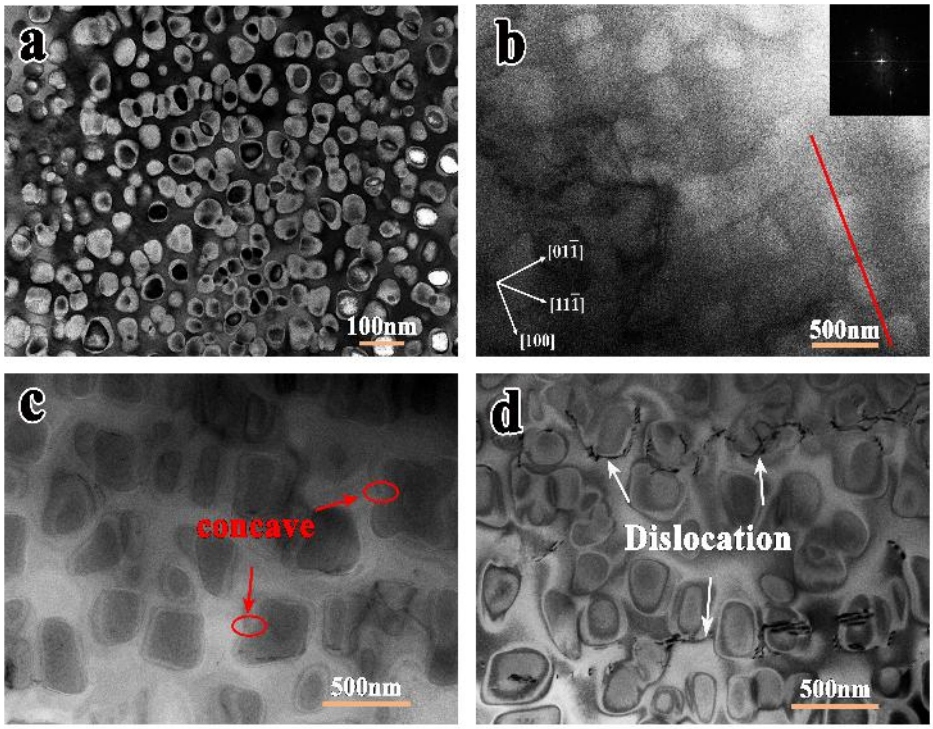

Fig. 9. The morphology and size distribution of γ′ phases: (a) AC and (b) FC; (c) and (d) the octets and cuboids γ′ phase under the cooling condition of FC.

The particle size distribution (PSD) of γ′ phases at the temperature of 1130 °C, with the soaking time of 30 h and under different cooling conditions, were obtained and shown in Fig. 10. It is found that the γ′ phases have the size range from 150 to 430 nm for the FC and 30 to 70 nm for the AC. The detailed particle size distribution analysis of 100 particles reveals a unimodal distribution for the FC and AC condition, as shown in Fig. 10(c) and (d). The size of γ′ phases was determined based on TEM images. For the spherical or near-spherical γ′ phases, the size is the equivalent diameter; while for cubic, octets and irregular γ′ phases, the size is the mean of the length and the width. The size distribution of γ′ phases mainly distributes in the range from 230 to 330 nm (64%) when the cooling condition is FC. When the cooling condition is AC, the size distribution of γ′ phases mainly distributes around 45 nm (45%) and

55 nm (42%). It reveals that the faster cooling rate is beneficial to obtain the fine γ′ phases and a more uniform size distribution.

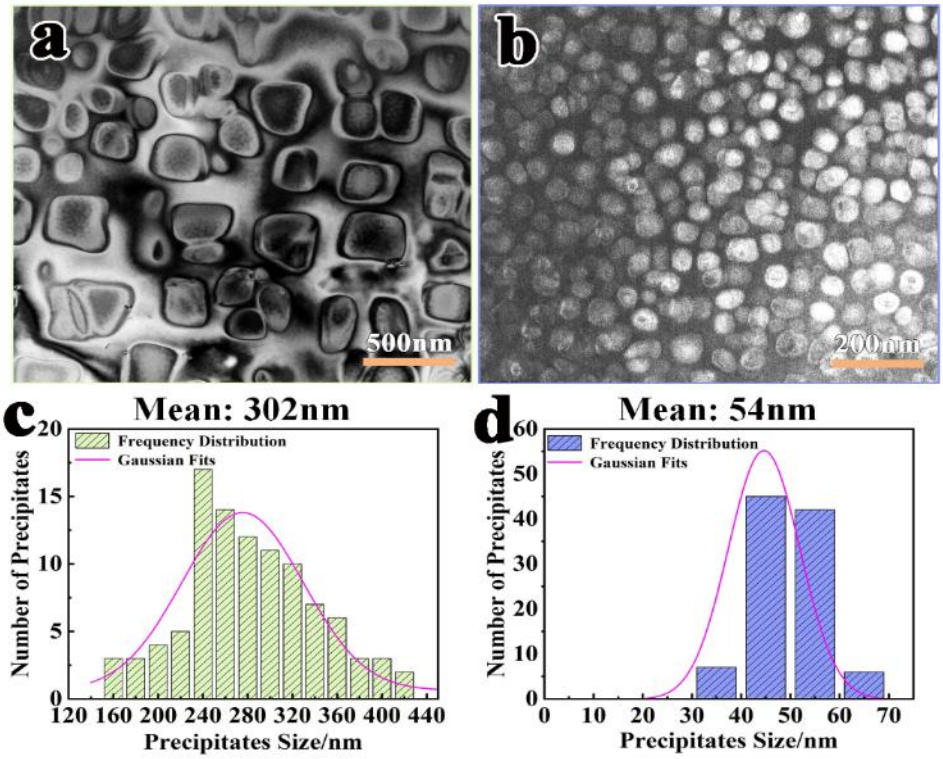

Fig. 10. The γ′ phases at the temperature of 1130 ℃ with the soaking time of 30 h under different cooling conditions: (a) FC; (b) AC; (c) and (d) the number of precipitates-size histograms of γ′ phases in (a) and (b) respectively.

4. Discussion

4.1 Re-precipitation mechanism of the γ′ phase with sphere, near-sphere, cubic, octets and finally-dendrites shape

The detailed experimental results show that the influence of the cooling condition is predominant to the morphology evolution of the re-precipitation γ′ phases. In this research, the γ′ phase morphology was transformed from spheres to near-sphere, and further changed to cubic and octets with concave faces, and finally became rather complex structures like

dendrites under various cooling conditions. The process of the morphology evolution of γ′ phase is schematically illustrated in Fig. 11. It is found that the primary γ′ precipitates in the as-received alloy kept a butterfly shape. Upon homogenizing treatment at γ′ super-solvus temperatures, the primary γ′ precipitate dissolution was completely done, as shown in Fig. 2(b). The secondary γ′ phase re-precipitation started from a sphere shape under fast cooling condition (AC). The γ′ phases got coarse, and changed from sphere to near-spherical shapes at SC. When the cooling condition was FC, the γ′ phases get coarsened very rapidly and grew irregularly, transformed to cuboids, octets with concave faces, and finally the dendrites. The coherent strain energy has a great effect on the evolution of the γ′ phases shape. In fact, the γ′ phases are mainly sphere since the anisotropic coherent strain energy can be negligible when the lattice misfit is small. When γ′ phases get coarse, the coherent strain energy was increased and the γ′ phases were transformed to cubic and octets with concave feature. The size of the γ′ phases was found to be larger, as shown in Fig. 10(c). This reveals that when the magnitude of the misfit is small, the γ′ phases must grow to a larger size before the cuboids or octets shape is formed. The research done by A. Maheshwari et al. [33] showed that the sphere γ′ phases firstly underwent Ostward ripening when the γ′ phases get coarse. The influence of the strain energy was thus predominant. The lattice mismatch was also ultimately responsible for strong spatial correlations during coarsening. Fig. 12(a) shows a high-resolution TEM image of the γ/γ′ interface, indicating a good coherence of the interface between γ matrix and γ′ phase. The inserts of Fig. 12(b) and (d) show the Fast Fourier Transformation (FFT) of the HR-TEM images. It can be seen that the interplanar spacing of γ matrix was different from that of the γ′ phase leading to the lattice misfit in the γ/γ′ interface, as shown in Fig. 12(c) and (e). These

correlations exist through elastic interaction energy, and significantly influence the microstructure of the aged Ni-based superalloys, leading to the dramatic alignment of γ′ phases along elastically soft <100> directions [34], as shown in Fig. 9(b).

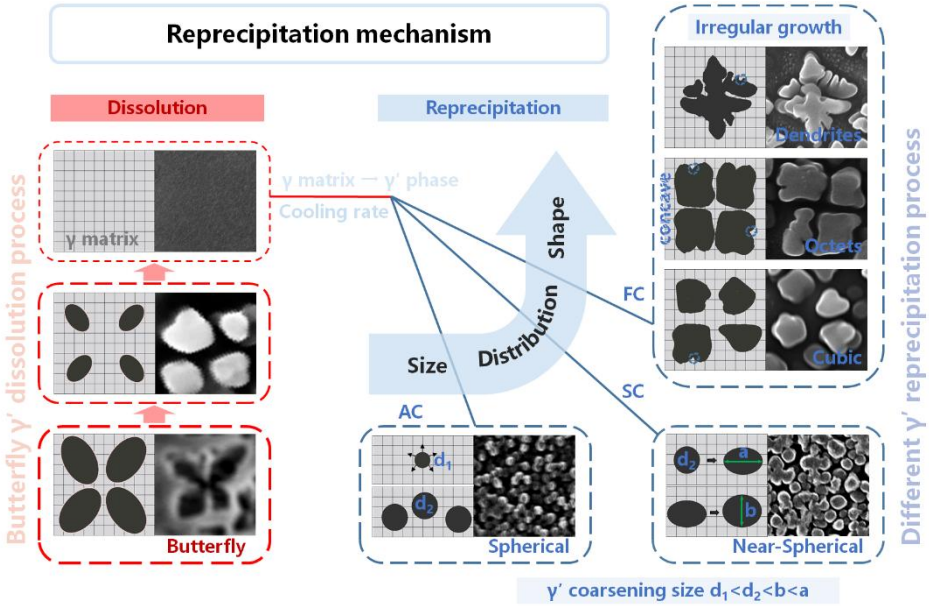

Fig. 11. The re-precipitation mechanism of the γ′ phases with sphere, near-sphere, cubic, octets and finally dendrites shape under various cooling conditions.

The low nucleation density and the sufficient diffusivity between γ′ phase and γ matrix are other essential factors for irregular growth of γ′ phase under slow cooling condition (FC). Yoo and Doherty [35, 36] concluded that the isotropic interfacial energy, the low lattice mismatch between the two phases, and a low density of nucleation for the formation of protrusions lead to the irregular growth of γ′ phase. Fig. 12(f) shows the HAADF image and the EDS map of the γ′ phases. It reveals that the secondary γ′ precipitate was rich in Ni, Al and Ti, while poor in Cr and Co. Since the atomic sizes of Al and Ti are 15% and 18% larger than that of Ni, respectively [37], the difference in the element content and atom size are also closely related to the γ′ phase shape.

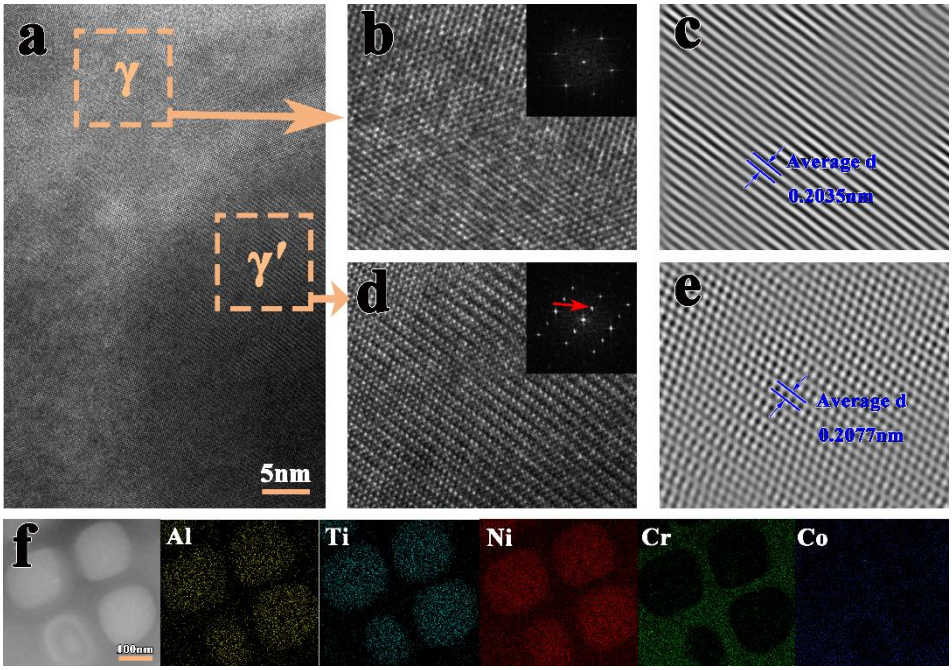

Fig. 12. High-resolution TEM image of the sample cooled at a slow cooling rate (FC): (a) high-resolution TEM image of the γ/γ′ interface; (b) and (d) high-resolution TEM image of γ and γ′, respectively, the insets of (b) and (d) show the FFT of the HR-TEM images and the zone axis is [011]; (c) and (e) show the IFFT of the HR-TEM images of γ and γ′, respectively; (f) HAADF image and the EDS map of the γ′ phases.

4.2 Morphological stability of the γ′ phase under FC and AC cooling condition

In this research, the irregular growth of γ′ phases at the slow cooling (FC) was observed and shown in Fig. 11. To simplify the analysis, it is assumed that there are negligibly small elastic strain energy, isotropic interface properties, relatively small composition change in the matrix during the re-precipitation, and local equilibrium at the interface in the process. The irregular growth of γ′ phases was thus analyzed based on the Mullins and Sekerka (MS) model [38]. In the model, the critical value ($R_c(L)$) was defined by the radius of the spherical particles:

$$\mathrm{Rc(L)} = \{(1/2)(L+1)(L+2)+1\}R^* \quad (1)$$

where L is the number of protrusions, $R^{*}= 2\Gamma_D/S$. The quantity R^{*} is the critical nucleation radius (corresponding to $C_R=C_\infty$) above which the sphere itself grows; while below which it shrinks. With $S= (C_\infty–C_0)/ C_0$ referring to supersaturation, C_∞ is the initial solute concentration in the supersaturated matrix, and C_0 is the equilibrium solute concentration at the precipitate/solid solution interface. $\Gamma_D= \sigma\Omega/RT$ showing capillary constant, which is a key factor determining the stability; σ is the γ/γ′ interfacial energy, and Ω is the increment of precipitate volume per mole of added solute; R is the gas constant, and T is the absolute temperature. Using σ and Ω values for superalloys reported by Ricks [39], the value of Γ_D was determined to be 9.7×10^{-4} μm. In addition, F. Masoumi et al [31] investigated the kinetics and mechanisms of γ′ reprecipitation in AD730 alloy and the maximum value of 0.4 for supersaturation constant 'S' was obtained by using the Thermo-calc® software. In this paper, the composition of the experimental superalloy is similar to AD730 alloy, and therefore, the value of S was determined to be 0.4.

The number of protrusions, L, was 4 for the specimens under slow cooling condition (FC). Using the above data and Eq. (1), the critical radius of the γ′ phase re-precipitation from γ′ super-solvus temperature under slow cooling rate (FC) was calculated to be 77.6 nm. In tandem with these analyses, the shape change of the γ′ phase critical radius versus supersaturation in this alloy was observed under various conditions and shown in Fig. 13. It reveals that the γ′ phases are stable below the critical radius; while instable above the critical radius. The γ′ phase growth trajectories for fast cooling (AC) and slow cooling (FC) conditions are schematically shown by Path-1 and Path-2, respectively. Under the slow cooling condition (FC), the γ′ phase re-precipitation from T_s is represented by Path-2 and the

nucleation density is low. The γ′ phases grow with the increasing supersaturation into the unstable region, and it thus has an irregular growth to the octets or dendritic shape. If the slowly cooled samples are isothermally aged at the high temperature, the octets or dendritic shape phases may be partially dissolved. These phases will have a transition to spherical precipitate by a relatively slow coarsening process. The process of splitting up or completion of the splitting process of γ′ phases under FC condition provides some evidences for this result. This phenomenon has a good agreement with the results obtained by Chen [40], who found that with the γ′ phase initially grew and then split into the smaller spherical phases. Of course, morphological instability should be decreased once the level of supersaturation is decreased. However, Fig. 3(a) reveals that the γ′ phase still keeps morphological instable. The reason is probably that most of the supersaturation is consumed for the nucleation of the third γ′ precipitates, rather than for the growth of secondary γ′ precipitates. Moreover, it shows that the γ′ phases are formed with the increasing supersaturation, and grow rapidly due to the high diffusion at high temperature, leading to the irregular shapes or morphological instability.

In addition, as shown by Path-2 in Fig. 13, it reveals that the octets with concave γ′ phases are formed in the unstable zone. Fan et al. [37] revealed that cuboidal γ′ phase exhibits protrusions in <111> directions, and the growth rate at these corners is faster than that at the center of the {100} planes, resulting in the morphology of γ′ phase transition from cuboid to concave shapes. In fact, the γ/γ′ interface curvature is negative in the concave region such that, the concave has a high strain energy, and causes the octets with the concave γ′ phase dissolution. This splitting process is favored thermodynamically [22].

In contrast, the effect of fast cooling condition (AC) on T_s is represented by Path-1 in Fig.

13 and the morphological instable is prevented. Under fast cooling condition (AC), the high number of fine γ′ phase is formed. A few nuclei formed at the temperature close to T_s grow with the increasing supersaturation. Fast cooling condition results in the increasing undercooling below the γ′-solvus temperature, which facilitates the nucleation of γ′ phase. Moreover, the supersaturation is quickly decreased because of the overlap of the diffusion fields. This overlapping inhibits the instable growth of γ′ phases and the spherical shape γ′ phases are formed. On the other hand, a mass of tiny γ′ phases are randomly distributed in the matrix since the interfacial energy is predominant under fast cooling condition (AC).

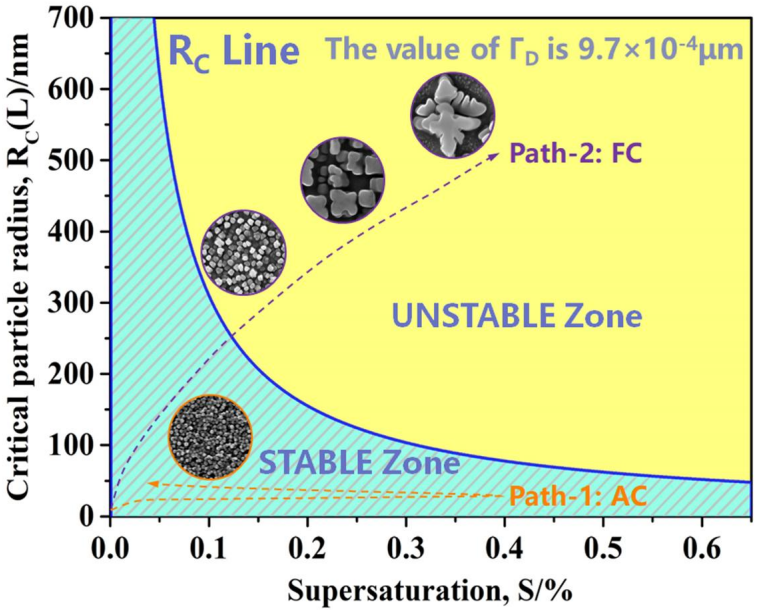

Fig. 13. The morphological stability of the re-precipitation γ′ phase under FC and AC cooling condition

5. Conclusions

In this work, the homogenization treatment of an as-cast Ni-based superalloy was conducted at γ′ super-solvus temperature under various conditions to investigate the morphology and size distribution of the re-precipitation γ′ phases. The re-precipitation mechanism of the γ′ phase in the as-cast Ni-based superalloy during the homogenizing

396 treatment was identified. Through extensive observation and analyses, the concluding remarks
397 are summarized in the following:
398 (1) The homogenization temperature and soaking time are closely related to the size
399 distribution of the γ′ phases. The mean size become larger and the distribution is more
400 uniform with the increase of the homogenization temperature or soaking time.
401 (2) Depending on cooling conditions, the γ′ phase morphology is transformed from sphere to
402 near-spherical, cubic, octets with concave features and finally dendrites. The γ′ phase size
403 is increased while the nucleation density is decreased with the cooling methods changed
404 from AC to FC.
405 (3) The re-precipitation mechanism of the γ′ phase with sphere, near-sphere, cubic, octets and
406 finally-dendrites shape under various cooling conditions was identified. The γ′ phase got
407 coarsening and irregular growth during different re-precipitation process.
408 (4) The γ′ phase shows the morphological instability under which re-precipitation is
409 generated from a refine spherical shape at the fast cooling condition (AC); while
410 irregularity growth even splitting happening at the slow cooling condition (FC) since the
411 supersaturation is sufficiently built up.

412 ## Acknowledgements

413 The work is financially supported by the National Natural Science Foundation of China
414 (Grant No. 51775440), the National Key Research and Development Program of China and
415 Fundamental Research Funds for the Central Universities. Also, Dr. Y.Q. Ning would like to
416 thank the funding support by the Hong Kong Scholar Program in The Hong Kong Polytechnic
417 University.

References

[1] R.C. Reed, The Superalloys: Fundamentals and Applications, Cambridge University Press, Cambridge 2006. https://doi.org/10.1017/CBO9780511541285.

[2] Y.Q. Ning, Z.K. Yao, M.W. Fu, H.Z. Guo, Dynamic recrystallization of the hot isostatically pressed P/M superalloy FGH4096 in hot working process, Mater. Sci. Eng. A. 527 (2010) 6968-6974. https://doi.org/10.1016/j.msea.2010.07.018.

[3] R. Radis, M. Schaffer, M. Albu, Multimodal size distributions of γ′ precipitates during continuous cooling of UDIMET 720 Li, Acta Mater. 57 (2009) 5739-5747. https://doi.org/10.1016/j.actamat.2009.08.002.

[4] Y.Q. Ning, Z.K. Yao, H.Z. Guo, M.W. Fu, Investigation on hot deformation behavior of P/M Ni-base superalloy FGH96 by using processing maps, Mater. Sci. Eng. A. 527 (2010) 6794-6799. https://doi.org/10.1016/j.msea.2010.07.040.

[5] Y.Q. Ning, Z.K. Yao, Y.Y. Lei, H.Z. Guo, M.W. Fu, Hot deformation behavior of the post-cogging FGH4096 superalloy with fine equiaxed microstructure, Materials Characterization. 62 (2011) 887-893. https://doi.org/10.1016/j.matchar.2011.06.004.

[6] S.S. Xiang, S.C. Mao, H. Wei, Selective evolution of secondary γ′ precipitation in a Ni-based single crystal superalloy both in the γ matrix and at the dislocation nodes, Acta Mater. 116 (2016) 343-353. https://doi.org/10.1016/j.actamat.2016.06.055.

[7] J.C. Zhang, L. Liu, T.W. Huang, Coarsening Kinetics of γ′ Precipitates in a Re-Containing Ni-based Single Crystal Superalloy during Long-Term Aging, Journal of Materials science & Technology. 62 (2021) 1-10. https://doi.org/10.1016/j.jmst.2020.05.034.

[8] B. Alabbad, L.H. Li, S. Tin, Controlling the grain boundary morphology and secondary γ′ precipitate

size distribution in Ni-base superalloys, Journal of Alloys and Compounds. 775 (2019) 931-941. https://doi.org/10.1016/j.jallcom.2018.10.031.

[9] S. Behrouzghaemi, R.J. Mitchell, Morphological changes of γ′ precipitates in superalloy IN738LC at various cooling rates, Mater. Sci. Eng. A. 498 (2008) 266-271. https://doi.org/10.1016/j.msea.2008.07.069.

[10] B. Wahlmann, F. Galgon, A. Stark, Growth and coarsening kinetics of gamma prime precipitates in CMSX-4 under simulated additive manufacturing conditions, Acta Mater. 180 (2019) 84-96. https://doi.org/10.1016/j.actamat.2019.08.049.

[11] F. Masoumi, M. Jahazi, D. Shahriari, Coarsening and dissolution of γ′ precipitates during solution treatment of AD730™ Ni-based superalloy: Mechanisms and kinetics models, Journal of Alloys and Compounds. 658 (2016) 981-995. https://doi.org/10.1016/j.jallcom.2015.11.002.

[12] Y.S. Yoo, D.Y. Yoon, M.F. Henry, The effect of elastic misfit strain on the morphological evolution of γ′-precipitates in a model Ni-base superalloy, Met. Mater. 1 (1995) 47-61. https://doi.org/10.1007/BF03055324.

[13] Y.J. Zhang, Y.J. Huang, L. Yang, Evolution of microstructures at a wide range of solidification cooling rate in a Ni-based superalloy, Journal of Alloys and Compounds. 570 (2013) 70-75. https://doi.org/10.1016/j.jallcom.2013.03.085.

[14] J. MacSleyne, M.D. Uchic, J.P. Simmons, Three-dimensional analysis of secondary γ′ precipitates in René-88 DT and UMF-20 superalloys, Acta Mater. 57 (2009) 6251-6267. https://doi.org/10.1016/j.actamat.2009.08.053.

[15] M.Z. Li, J. Coakley, D. Isheim, Influence of the initial cooling rate from γ′ supersolvus temperatures on microstructure and phase compositions in a nickel superalloy, Journal of Alloys and Compounds.

462 732 (2018) 765-776. https://doi.org/10.1016/j.jallcom.2017.10.263.
463 [16] Y.Y. Qiu, The effect of the lattice strains on the directional coarsening of γ′ precipitates in Ni-based
464 alloys, J. Alloys Compd. 232 (1996) 254-263. https://doi.org/10.1016/0925-8388(95)01914-6.
465 [17] P. Pandey, S. Kashyap, D. Palanisamy, On the high temperature coarsening kinetics of γ′ precipitates
466 in a high strength Co37.6Ni35.4Al9.9Mo4.9Cr5.9Ta2.8Ti3.5 fcc-based high entropy alloy, Acta Mater.
467 177 (2019) 82-95. https://doi.org/10.1016/j.actamat.2019.07.011.
468 [18] N. Zhou, C. Shen, M.J. Mills, Phase field modeling of channel dislocation activity and γ′ rafting in
469 single crystal Ni-Al, Acta Mater. 55 (2007) 5369-5381. https://doi.org/10.1016/j.actamat.2007.06.002.
470 [19] W.H. Sun, S.L. Cui, L.J. Zhang, Phase-field Simulation of Microstructural Evolution of γ Precipitate
471 in γ′ Matrix in Binary Ni-Al Alloys, Procedia Engineering. 36 (2012) 200-206.
472 https://doi.org/10.1016/j.proeng.2012.03.031.
473 [20] J.Z. Zhu, T. Wang, A.J. Ardell, Three-dimensional phase-field simulations of coarsening kinetics of γ′
474 particles in binary Ni-Al alloys, Acta Mater. 52 (2004) 2837-2845.
475 https://doi.org/10.1016/j.actamat.2004.02.032.
476 [21] E.D. Wu, G.G. Sun, B. Chen, A neutron diffraction study of lattice distortion, mismatch and
477 misorientation in a single-crystal superalloy after different heat treatments, Acta Mater. 61 (2013)
478 2308-2319. https://doi.org/10.1016/j.actamat.2013.01.001.
479 [22] P. Cha, D. Yeon, S. Chung, Phase-field study for the splitting mechanism of coherent misfitting
480 precipitates in anisotropic elastic media, Scr. Mater. 52 (2005) 1241-1245.
481 https://doi.org/10.1016/j.scriptamat.2005.02.026.
482 [23] A.R.P. Singh, S. Nag, J.Y. Hwang, Influence of cooling rate on the development of multiple
483 generations of γ′ precipitates in a commercial nickel base superalloy, Materials Characterization. 62

(2011) 878-886. https://doi.org/10.1016/j.matchar.2011.06.002.

[24] S.S. Babu, M.K. Miller, J.M. Vitek, Characterization of the microstructure evolution in a nickel base superalloy during continuous cooling conditions, Acta Mater. 49 (2001) 4149-4160. https://doi.org/10.1016/S1359-6454(01)00314-7.

[25] J.Y. Hwang, R. Banerjee, J. Tiley, Nanoscale Characterization of Elemental Partitioning between Gamma and Gamma Prime Phases in René 88 DT Nickel-Base Superalloy, Metall. Mater. Trans. A. 40 (2008) 24-35. https://doi.org/10.1007/s11661-008-9691-2.

[26] R. Radis, M. Schaffer, M. Albu, Multimodal size distributions of γ′ precipitates during continuous cooling of UDIMET 720 Li, Acta Mater. 57 (2009) 5739-5747. https://doi.org/10.1016/j.actamat.2009.08.002.

[27] J.Y. Hwang, S. Nag, A.R.P. Singh, Compositional Variations between Different Generations of γ′ Precipitates Forming during Continuous Cooling of a Commercial Nickel-Base Superalloy, Metall. Mater. Trans. A. 40 (2009) 3059-3068. https://doi.org/10.1007/s11661-009-0075-z.

[28]J.L. Xu, X.F. Xie, Z.N. Bi, Hot deformation characteristics and dynamic recrystallization mechanism of GH4730 Ni-based superalloy, Journal of Alloys and Compounds. 785 (2019) 918-924. https://sci-hub.se/10.1016/j.jallcom.2019.01.237.

[29] A. Devaux, E. Georges, P. Héritier, Development of new C&W superalloys for high temperature disk applications, Advanced Materials Research. 278 (2011) 405-410. https://doi.org/10.1002/9781118495223.ch16.

[30] A. Devaux, E. Georges, AD730™–A new nickel-based superalloy for high temperature engine rotating parts, Superalloys 2012, TMS (The Minerals, Metals & Materials Society). (2012) 911-919. https://doi.org/10.1002/9781118516430.ch100.

506 [31] F. Masoumi, D. Shahriari, M. Jahazi, Kinetics and Mechanisms of γ′ Reprecipitation in a Ni-based
507 Superalloy, Scientific Reports. 6 (2016) 28650. https://doi.org/10.1038/srep28650.
508 [32] A. Breidi, J. Allen, A. Mottura, First-principles modeling of superlattice intrinsic stacking fault
509 energies in Ni_3Al based alloys, Acta Mater. 145 (2018) 97-108.
510 https://doi.org/10.1016/j.actamat.2017.11.042.
511 [33] A. Maheshwari, A.J. Ardell, Morphological evolution of coherent misfitting precipitates in anisotropic
512 elastic media, Physical Review Letters. 70 (1993) 2305-2308.
513 https://doi.org/10.1103/physrevlett.70.2305.
514 [34] A.J. Ardell, R.B. Nicholson, On the modulated structure of aged Ni-Al alloys: with an Appendix On
515 the elastic interaction between inclusions by J. D. Eshelby‡‡Cavendish Laboratory, University of
516 Cambridge, England, Acta Metall. 14 (1966) 1295-1309.
517 https://doi.org/10.1016/0001-6160(66)90247-1.
518 [35] Y.S. Yoo, Morphological instability of spherical γ′ precipitates in a nickel base superalloy, Scr. Mater.
519 53 (2005) 81-85. https://doi.org/10.1016/j.scriptamat.2005.03.022.
520 [36] R.D. Doherty, Role of interfaces in kinetics of internal shape changes, Metal Science. 16 (1982) 1-14.
521 https://doi.org/10.1179/030634582790427019.
522 [37] X.Q. Fan, Z.P. Guo, X.F. Wang, Morphology evolution of γ′ precipitates in a powder metallurgy
523 Ni-base superalloy, Materials Characterization. 139 (2018) 382-389.
524 https://doi.org/10.1016/j.matchar.2018.02.038.
525 [38] W.W. Mullins, R.F. Sekerka, Morphological stability of a particle growing by diffusion or heat flow, J.
526 Appl. Phys. 34 (1963) 323-329. https://doi.org/10.1007/978-3-642-59938-5_4.
527 [39] R.A. Ricks, A.J. Porter, R.C. Ecob, The growth of γ′ precipitates in nickel-base superalloys, Acta

528 Metall. 31 (1983) 43-53. https://doi.org/10.1016/0001-6160(83)90062-7.

529 [40] Y.Q. Chen, R. Prasath babu, Thomas J.A. Slater, An investigation of diffusion-mediated cyclic

530 coarsening and reversal coarsening in an advanced Ni-based superalloy, Acta Mater. 110 (2016)

531 295-305. https://doi.org/10.1016/j.actamat.2016.02.067.